Indian Journal of Geo Marine Sciences
Vol. 48 (06), June 2019, pp. 857-866

A frequency-domain full waveform inversion method of elastic waves in quantitative defection investigation

Jundong Chen[1,2], Huan Wang[3], Danqing Song[2*], & Xiurun Ge[2]

[1]China Railway Academy Co., Ltd, Chengdu 611731, China

[2]School of Naval Architecture, Ocean and Civil Engineering, Shanghai Jiao Tong University, Shanghai 200040, China

[3]Shanghai Urban Construction municipal engineering (group) CO. LTD, Shanghai-200070, China

*[E-mail: 316831928@qq.com]

Received 14 November 2017; revised 11 May 2018

Full waveform inversion is a challenging data-fitting procedure based on full wave field modeling to extract quantitative information on elastic properties of subsurface structures. We developed a frequency-domain full-waveform inversion method of elastic waves for stratified media, adopting a quasi-linearization method coupled with a random search algorithm. The inversion process of this method is irrelevant to hypocenter function and can be considered as a kind of combination between the heuristic and non-heuristic inversion methods. To verify our method, we apply it to three numerical two-dimensional models with different intermediate structures (dipping, arched and hollow), and their structures are well revealed. With some pretreatments on response waveforms, such as filtering, normalization and correlation analysis, the full-waveform inversion method is extended to models with damaged area and its feasibility and accuracy verified. Alignment of full waveform inversion method and its cost of computing, several strategies exist to treat this quantitative detecting problem. In Chengdu-Chongqing guest emergency project, the application of full waveform inversion method saves a lot of time. In this method, each section only needs 2 detectors and only need to be hammered twice, while the traditional CT (Computed Tomography) test requires 11 detection filters and at least 11 hammering, and each section has 121 waveform data. In some cases, we can obtain some important priori information through field investigation. The priori information can be used to accelerate the inversion process.

[**Keywords:** Full waveform inversion; Stratified media; Quantitative elastic parameters; Quasi-linearization method; Random search]

Introduction

In geotechnical engineering investigation and detection, the full waveform inversion is a type of nondestructive and quantitative method used for grasping the physical properties of structures. It has been gradually adopted in geotechnical engineering in the past several decades and has drawn more and more attention[1]. The elastic wave is one of the most commonly used forms in the full waveform inversion method. When the elastic wave passes through the target medium, the elastic property information of the materials will be carried by the waveforms. By various inversion approaches, this method attempts to match the elastic parameters of the target medium from the received waveforms data by comprehensively utilizing the amplitude, travel time, phase and dispersion. In connection with the development of data acquisition technique, it has become important to investigate highly contrasted layered media intersected by the inversion method. With the increasing resolution of seismic observations and the use of multi-component detectors, there is a growing awareness that the importance of the full waveform inversion is increasing considerably[2,3]. Grechka *et al*. (1999), for example, had successfully reached the anisotropy parameters of the soil medium by combining the P-wave and P-SV wave inversion[4]. Romdhane *et al*. (2011) performed the full-waveform inversion algorithm involving both body and surface waves for near-surface investigation of a small-scale model[5].

The full waveform inversion problem is non-linear at most, and the inversion method is one critical issue of the full waveform inversion. The solution of this non-linear inversion problem is the process of optimization for a designated objective function (or probability density)[6]. To minimize the error of the fit between the recorded and the modeled data, the initial model of the target structure must be improved; many algorithms have been developed for this

optimization. There have been a number of studies simplifying the non-linear inversion problem by various linear methods, such as the transfer matrix[7], Born approximate method[8], Rytov approximate method[9], and Radon transform approximation method[10]. Although the computational cost is greatly reduced by linear simplification, the accuracy and feasibility are lacking because of the strictly approximate premises.

Profited by the development of advanced computer technology, nonlinear inversion algorithms for full waveform inversion have been rapidly promoted. They perform with acceptable computational costs and show much better accuracy, feasibility and anti-noise capabilities. The nonlinear algorithms used in full waveform inversion are divided into two categories. The first is non-heuristic algorithms, such as the steep descent method[11], Gauss-Newton method[12,13], conjugate gradient methods[14], quasi-linear iterative-optimization approach[15], and so on. The non-heuristic algorithms focus on local linearization of the objective function based on its partial differential characteristics. It has the advantages of good convergence, rapid computation speed and uniqueness of solution, but it strongly relies on the initial model and is very susceptible to falling into local minimums. During the inversion procedure, if the initial model is not well established and is located outside the best convergence region due to inadequate prior information, the global optimal solution is difficult to reach as a result[16].

The other category is heuristic algorithms. These algorithms fix attention on intelligently searching for the global optimal solution. Many studies come from the intersection between modern science disciplines; not only mathematics, geophysics and seismology, but also biochemistry and statistics. The Monte-Carlo method[17,18] is based on the heuristic random search and possesses the nature of gambling. The Simulated Annealing Method[19,20] is based on combinatorial optimization in statistical testing. Artificial Neural Network[21,22] is a class of artificial intelligence algorithms and is sometimes coupled with signal processing. Genetic Algorithms[23,24] are a type of stochastic algorithm for simulating the process of natural selection and mutation. The heuristic algorithms avoid the derivative operator of an objective function, thus their dependence on the initial model is reduced and they possess wide adaptability. However, the heuristic algorithms also have the disadvantages of high computational cost, low convergence and poor uniqueness of solution. Geophysicists and applied mathematicians also seek settlements by combining the above two algorithms to mitigate the requirements on the initial model, improve the computational efficiency and achieve a global optimal solution as frequently as possible[25,26,27].

In the present work, we develop a frequency-domain full-waveform inversion method of elastic waves for stratified media. The quasi-linearization method is adopted, coupled with the random search algorithm, which can be considered as a type of combination between non-heuristic and heuristic inversion algorithms. As one of the non-heuristic algorithms, the quasi-linearization method iteratively calculates the Jacobian matrix for inversion, instead of the Hessian matrix, and improves the initial model by principles of steepest descent. The random search algorithm comes from the Monte-Carlo method, and it will help the inversion process escape from local minima within the appropriate search scope. At last, we will reach a certain number of minimums and find the most suitable one as the global minimum. Assuming that the prior information is sufficient, and the model is described by a simple model with a limited number of elastic parameters to be extracted, our full waveform inversion algorithm is quantitative and suitable for computation on PC. In the case study, we apply it to three numerical two-dimensional (2D) models with different intermediate structures (dipping, arched and hollow). At the beginning of the inversion computation, the waveforms' acquisition geometry and the considered frequency bandwidth are specially considered, and then the three types of intermediate structures are well revealed, respectively. Furthermore, we extend it to two three-dimensional (3D) stratified media models. One is a homogenous stratified model, and the other one is a stratified model with a defect area. A series of pre-treatments and proper inversion strategies are adopted into the response waveforms from the 3D models. At last, the distribution of the defect area is clearly evaluated and the feasibility and accuracy of our algorithm is verified in this 3D quantitative problem.

Alignment of full waveform inversion method and its cost of computing, the inversion method together with the test method is applied to a emergency project, in which the 3D models are replaced with multiple 2D models; the results show that the method requires less time than that in the traditional CT test.

Materials and Methods

We combine the quasi-linear method (QLM) in the frequency domain with the random search algorithm (RSA) as the inversion method in our work. The inversion method as well as its inverse steps and terminal conditions are discussed in detail in this section.

Quasi-linear method in the frequency domain

According to the deconvolution algorithm proposed by Ernst *et al*. 2007[28], the response waveforms in a given model caused by a given hypocenter can be calculated by the convolution operation between the hypocenter function and model response function. Because the convolution operation is converted to multiplication in the frequency domain, the frequency spectrum of the response waveform is formulated as

$$\boldsymbol{F}_j^f = \boldsymbol{\varphi}^f \times \boldsymbol{M}_j^f, \ (j = 1,2,3,\cdots,m) \quad \ldots (1)$$

where '×' is the convolution operation, the superscript '*f*' represents the frequency domain, $\boldsymbol{F}_j^f$ is the frequency spectrum on the j^{th} detector, m is the number of detectors, φ is the hypocenter function and $\boldsymbol{M}$ is the response function of the model.

Then, we create a new vector $\boldsymbol{G}_j$, irrelevant for hypocenter function, by dividing the frequency spectrum on the $(j+1)^{\text{th}}$ detector by the frequency spectrum on the j^{th} detector, as shown in Eqn (2). Generally, to avoid the divergence caused by a near-zero divisor, a slight white noise should be added to each divisor.

$$\boldsymbol{G}_j = \frac{\boldsymbol{F}_{j+1}^f}{\boldsymbol{F}_j^f} = \frac{\boldsymbol{\varphi}^f \times \boldsymbol{M}_{j+1}^f}{\boldsymbol{\varphi}^f \times \boldsymbol{M}_j^f} = \frac{\boldsymbol{M}_{j+1}^f}{\boldsymbol{M}_j^f}, \ (j = 1,2,3,\cdots,m-1) \quad \ldots (2)$$

Assuming that the matrix $\boldsymbol{G}^{\text{obs}}$ represents the observation data in the site and $\boldsymbol{G}$ represents the forward data of the simulated model, we thus define the 2-norm value of the difference as the objective function Q, which is expressed as Eqn (3). The destination is to find the correct model that makes the objective function Q as small as possible.

$$Q = \left\| \boldsymbol{G}^{\text{obs}} - \boldsymbol{G} \right\|_2 = \sum_{j=1}^{m-1} \left\| \boldsymbol{G}_j^{\text{obs}} - \boldsymbol{G}_j \right\|_2 = \sum_{j=1}^{m-1} \left\| \frac{\boldsymbol{M}_{j+1}^{f,\text{obs}}}{\boldsymbol{M}_j^{f,\text{obs}}} - \frac{\boldsymbol{M}_{j+1}^f}{\boldsymbol{M}_j^f} \right\|_2 \quad \ldots (3)$$

In the procedure of optimization, this generalized non-linear inverse problem is approximately linearized by Taylor series expansion and formulated as a linear system of equations; it can be rewritten as

$$\boldsymbol{A}\Delta\boldsymbol{x} = \boldsymbol{B}, \quad \ldots (4)$$

where $\boldsymbol{A}$ is the Jacobian matrix with a size of $n \times n$, $\Delta\boldsymbol{x}$ is the corresponding adjustment vector with a size of $n \times 1$, $\boldsymbol{B}$ is the coefficient vector, and n is the number of inversed parameters.

Because elements inside the matrix $\boldsymbol{A}$ and vector $\boldsymbol{B}$ are imaginary numbers, to ensure the real values of the solution $\Delta\boldsymbol{x}$ and consider the phase angles of response waveforms, it is necessary to separate the real part of each element from its imaginary part. Taking the operators of *RL*() and *IM*() as the real part and imaginary part of the elements, respectively, the elements in matrix $\boldsymbol{A}$ and vector $\boldsymbol{B}$ are obtained as follows:

$$A_{p,l} = \sum_{j=1}^{m-1} \left(RL\left(\frac{\partial \boldsymbol{G}_j}{\partial x_p}\right) \cdot RL\left(\frac{\partial \boldsymbol{G}_j}{\partial x_l}\right) + IM\left(\frac{\partial \boldsymbol{G}_j}{\partial x_p}\right) \cdot IM\left(\frac{\partial \boldsymbol{G}_j}{\partial x_l}\right) \right),$$

$$B_p = \sum_{j=1}^{m-1} \left(RL\left(\frac{\partial \boldsymbol{G}_j}{\partial x_p}\right) \cdot RL\left(\boldsymbol{\varepsilon}_j\right) + IM\left(\frac{\partial \boldsymbol{G}_j}{\partial x_p}\right) \cdot IM\left(\boldsymbol{\varepsilon}_j\right) \right).$$

$$(p,l = 1,2,3,\cdots,n) \quad \ldots (5)$$

where '.' is dot product calculation x_{i} is the i^{th} inversed parameter in the parameter vector $\boldsymbol{x}$ of the model, $\boldsymbol{\varepsilon}_j$ is the residual vector, and $\boldsymbol{\varepsilon}_j = \boldsymbol{G}_j^{\text{obs}} - \boldsymbol{G}_j$.

Generally, it is difficult or impossible to obtain an explicit expression of the forward data $\boldsymbol{G}$; the derivative quotient $\partial \boldsymbol{G}_j / \partial x_i$ inside Eqn (5) is replaced by the differential quotient, which is expressed as:

$$\frac{\partial \boldsymbol{G}_j}{\partial x_i} = \frac{\boldsymbol{G}_j(\boldsymbol{x} + \delta\boldsymbol{x}_i) - \boldsymbol{G}_j(\boldsymbol{x})}{\delta x_i} \ (j = 1,2,3,\cdots,m-1), (i = 1,2,3,\cdots,n) \quad \ldots (6)$$

where $\delta\boldsymbol{x}_{\text{i}}=(0, \ldots, \delta x_{\text{i}}, \ldots,0)^{\text{T}}$. It is a slight disturbance on the i^{th} objective parameter x_{i} in the parameter vector $\boldsymbol{x}$ and usually taken as 5 ~ 10% of x_{i}.

Because the Jacobian matrix $\boldsymbol{A}$ is symmetrical and positive, it can be improved by Tikhonov regularization[29,30]; as a result, the solution of linear Eqn. (4) is as below:

$$\Delta\boldsymbol{x} = (\boldsymbol{A} + a\boldsymbol{E})^{-1}\boldsymbol{B} \quad \ldots (7)$$

where a is the regularization parameter and is determined by Eqn (8) in each iteration:

$$a_k = (1/2)^k \, T_k^{\max}, \ (k = 1,2,3,\cdots) \quad \ldots (8)$$

where k is the iteration time and $T_k^{\max}$ is the maximum eigenvalue of the Jacobian matrix $\boldsymbol{A}$ in the k^{th} iteration.

By adding the adjustment vector $\boldsymbol{\Delta x}$, the parameter vector $\boldsymbol{x}$ is modified as $\boldsymbol{x}+\boldsymbol{\Delta x}$. The parameter vector $\boldsymbol{x}$ will be modified iteratively until the objective function Q reaches the terminal condition.

From the derivation above, it is observed that the inversion process is irrelevant to the hypocenter function. As a result, it can avoid the disadvantages during the data collection of the hypocenter. For some easier cases in which the model is described by a simple model with a limited number of unknown elastic parameters, the computational cost of the Jacobian matrix is acceptable and our full waveform inversion method is suitable for computation on PC. The quasi-linear method has advantages including finite iteration steps, calculation speed and relatively accurate solution, but it is highly dependent on the initial model and is easily trapped in local minima, which leads to improbability that it will find the optimal solution. Therefore, we adopt the random search algorithm, coupled with the quasi-linear method, to mitigate the disadvantages of the quasi-linear method.

Random search algorithm

The RSA is a type of heuristic algorithm, and it derives from the Monte-Carlo method. Based on various search radiuses, a model space is built and RSA tries stochastic models in it with the purpose of finding a suitable model that decreases the value of the objective function, Q. Because of its fast speed and global parameter consideration, RSA is very suitable for high-order nonlinear inversion problems with multi-parameters and multiple minima[31].

For a parameter vector $\boldsymbol{x}$ output by the program of QLM, if it belongs to a local minimum point, RSA is used for finding a new suitable parameter vector, and the new vector $\boldsymbol{x}$ is searched by the following equation:

$$x_{\text{new},i} = x_{\text{old},i} + (\text{sign}) \times \text{d}x_i \times \text{rand}, \quad \ldots (9)$$

in which $x_{\text{new, i}}$ and $x_{\text{old, i}}$ are the new and unmodified i^{th} parameters, respectively; 'sign' is the search direction and is equal to 1 or -1 with half probability; and $\text{d}x_{\text{i}}$ is the search radius of each parameter and is determined by prior information and empirical estimation. It is taken as 25% of x_{i} in this paper; 'rand' is a random number within the range of [0,1]. The search process will continue until the value of the objective function, Q decreases and the new parameter vector is taken as a new initial model of QLM. Repeat the above steps several times until the terminal condition is satisfied, and then output the last parameter vector as the global minimum result.

Terminal condition and steps

Two terminal conditions are designed for the iterations of the full waveform inverse method. If either of them is satisfied, the calculation will conclude.

The first one is related to the objective function. As Eqn (10) shows, when the objective function Q is less than a pre-set very small value, the difference between the observation data, $\boldsymbol{G}^{\text{obs}}$, and the forward data, $\boldsymbol{G}$, is considered as acceptable:

$$Q_k \le \eta_1 . \quad \ldots (10)$$

The second one concerns relative correction. Sometimes the adjustment vector, $\boldsymbol{\Delta x}$, is trapped in numerical oscillation; the iteration will stop in spite of the value of the objective function, Q remaining relatively large. In this state, the terminal condition is shown as below:

$$\sum_{i=k}^{k+a} \frac{Q_i - Q_{i-1}}{aQ_{i-1}} \le \eta_2 . \quad \ldots (11)$$

Here, η_1 and η_2 are pre-set small values and are determined by the accuracy requirement of the inversion. The subscript k represents the k^{th} iteration. The value 'a' ensures that the objective function, Q maintains stability for at least a iterations.

The steps of each iteration of our full waveform inversion method are:

(1) Seek an approximate initial model with parameter vector $\boldsymbol{x}_0$ on the basis of observation waveforms and auxiliary information in site;
(2) Based on the initial model $\boldsymbol{x}_0$, carry out the forward calculation and obtain the forward data matrix $\boldsymbol{G}^0$, and then calculate the residual matrix $\boldsymbol{\varepsilon}$, as well as the value of the objective function Q;
(3) By the solution of QLM, obtain the results of the parameter vector $\boldsymbol{x}$;
(4) Ascertain whether the terminal condition is satisfied. If not, carry out RSA programs to find a new parameter vector $\boldsymbol{x}$ and repeat Steps (2) and (3);
(5) If the terminal condition is satisfied, stop the calculation and output the parameter vector $\boldsymbol{x}$ as the last result.

The flow chart of the above iteration steps is shown in Figure 1.

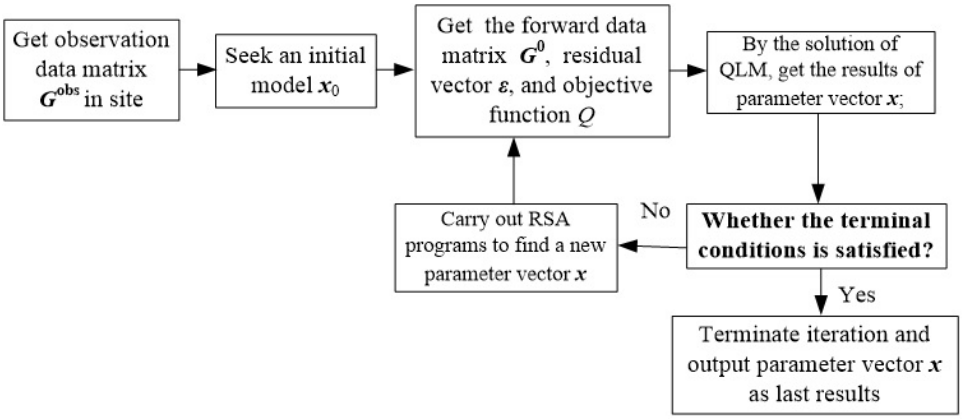

Fig. 1 — Flow chart of iteration steps of full waveform inversion

Numerical examples on a model

Modeling:

For verification, we apply the full waveform inversion method to a responsive waveform data set generated by 20 semi-infinite models. As Figure 2 shows, a models with damaged area is cast. It is assumed that the outer layer is considered to be concrete, the material of the damaged area is loose concrete, whose strength is relatively weak.

Some necessary artificial boundary conditions are imposed on the numerical boundaries in the models. The left and the right boundary condition are set to be free. The upper and the bottom boundary condition are set as a perfectly matched layer (PML) absorbing boundary[32,33]. Because the strains of materials in site testing are finite and small, the materials here are considered in the elastic domain. All of the elastic physical parameters are listed in Table 1, where ρ , V_p and V_s are the density, P-wave velocity and S-wave velocity of each material, respectively, and μ_d is the dynamic Poisson's ratio.

The hypocenter function used for the observation data, $\boldsymbol{G}^{obs}$ is an artificial signal of a hammer. The frequency spectrums of the artificial signal cover most of the hammer sources within 0.1~4 kHz. The waveform of the artificial signal in the time domain and its frequency spectrum are shown in Figure 3.

Inversion analysis

During the iterations, the hypocenter function in the forward calculation and its dominant frequency should be confirmed by the frequency spectrum of the observed waveforms collected in the site. Two seismic detectors are set on the left free boundary. By the finite-difference time domain (FDTD) method for elastic wave equations, the time-history curves of displacements on the two seismic detectors are recorded as response waveforms. The response waveforms in the time domain and their frequency spectrums are shown in Figures 4 and 5.

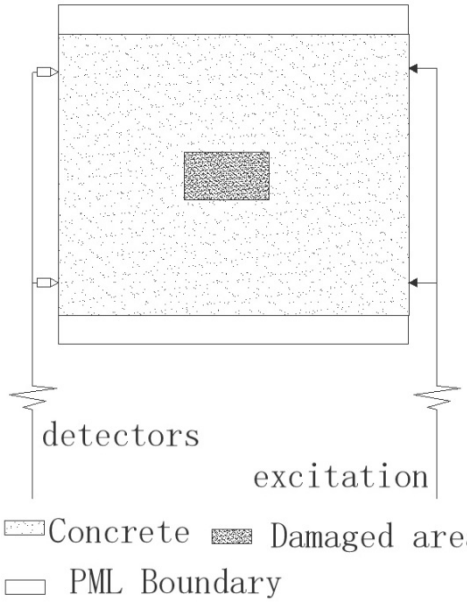

Fig. 2 — Model of the inversion example (models with damaged area)

Table 1—Material parameters in the numerical model

No.	Layer	ρ (kg/m^3)	V_p (m/s)	V_s (m/s)	μ_d
1	Concrete	2400	4500	2800	0.184
2	damaged area	100	800	400	0.333

As the frequency spectrums of the response waveforms are concentrated on the bands of 0.8 ~ 4 kHz, we choose the Ricker wavelet with main frequency of 2 kHz in the inverse process. The formula of the Ricker wavelet is:

$$U(t)=\frac{2}{\sqrt{3\sigma}\pi^{0.25}}(1-\frac{t^2}{\sigma^2})\exp(-\frac{t^2}{2\sigma^2}), \quad \ldots (12)$$

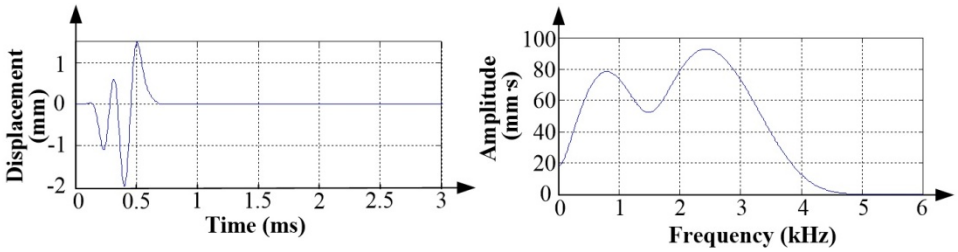

Fig. 3 — Hypocenter for the observation data in numerical examples: (a) Waveform in the time domain; (b) Frequency spectrum.

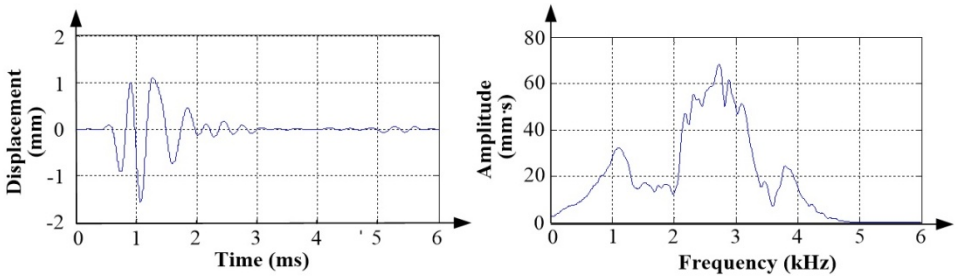

Fig. 4 — Response waveform on the first seismic detector on the upper free boundary: (a) Waveform in the time domain; (b) Frequency spectrum.

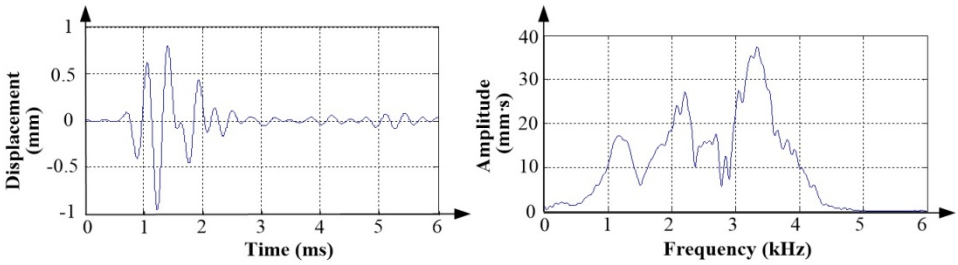

Fig. 5 — Response waveform on the second seismic detector on the upper free boundary: (a) Waveform in the time domain; (b) Frequency spectrum.

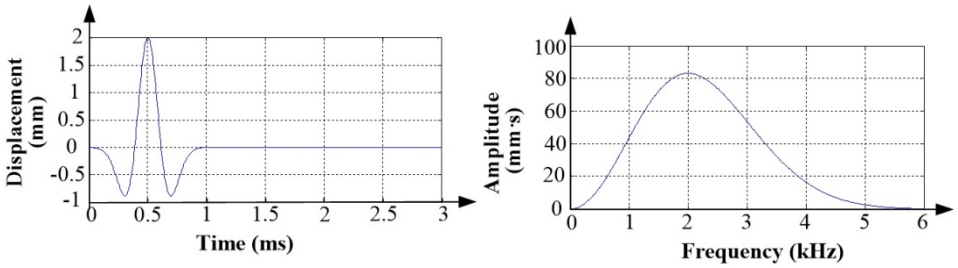

Fig. 6 — Waveform of the Ricker wavelet for the inverse calculation: (a) Waveform in the time domain; (b) Frequency spectrum.

where σ is the main frequency and is equal to 2000 here, t is the time and the sampling interval is 5 μs. Thus, the waveform of the Ricker wavelet in the time domain and its frequency spectrums are shown in Figrue 6.

Generally, as the P-wave of model is unknown, the models of media are adopted in the inverse calculation and P^0 is the projection of P-wave velocity of the model pixel are assumed as target parameters. The pre-set small values of the terminal condition are set as η_1=0.1 and η_2=0.01.

Here, we take the inversion work as an example, as shown in Figure 7. Given the initial values of v_p= 800 m/s, by our full waveform inversion method, the objective function values are decreased along with the iterations as shown in Figure 8. When either of the terminal conditions is satisfied, the iterations are halted and the last results of the parameters are P^0= 3160 m/s. Compared with the exact values, the relative error of the parameters are 5.4%. The final time-domain waveforms and observed waveforms are shown in Figure 9, and it is observed that the final

residual waveform between each other is almost negligible. It can be concluded that the convergence and accuracy of our full waveform inversion method in the frequency domain are acceptable and our algorithm is feasible for quantitatively revealing the unknown parameters of a 2D profile model on PC.

Bringing all of the results on the detection points on the entire surface of the defective model together, we obtain the profile of P-wave velocities of the entire numerical model and the distribution map of P-wave velocities (Fig. 9).

Field test

In July 2015, at the early stage of the combined operation of Chengdu-Chongqing passenger dedicated line, a total of 31 point pre-stressed continuous beams were found. The quality of the concrete at the bottom of the pier and the top of the pier was defective, as shown in Figure 10. For the effective and rapid completion of the inspection work, and to ensure the accuracy of test results, after careful discussions and research, we determined to adopt a combination of endoscope detection, full waveform inversion, and borehole to carry out special inspection.

Since the full waveform inversion method can reduce the time of field data acquisition, and the defective area can be identified quickly and efficiently, full waveform inversion method is adopted to detect the defects. The method is simple and quick, requiring only two receiving sensors. Each section only needs to be hit twice; the specific process of field detection is shown in Figure 11. It is worth noting that, in some cases, some site investigations are based on priori information, such as location, size and depth. In the inversion process, we use the information to define and initialize the parameters of the model, which will improve the retrieval speed to a great extent. The full waveform inversion technique is used to detect 31 points and the information of the defective area is acquired accurately and quickly.

Field inspection: The detection section arrangement fully considers the depth of the test concrete that may be affected by disease. At the same time, because the reinforced concrete will affect the accuracy of CT testing, the ultrasonic testing profile should try to avoid the steel-intensive area. Given the above two points, the concrete CT acoustic tomography detection will set section 3 along the beam height detection. Section 1 is 8 cm from the box girder bottom, section 2 16 cm and section 3 28 cm from the box girder bottom.

The detection section is a 7.5 m (transverse) * 2.0 m (longitudinal) rectangular plane, one measuring point for acoustic emission line layout, numbered F1

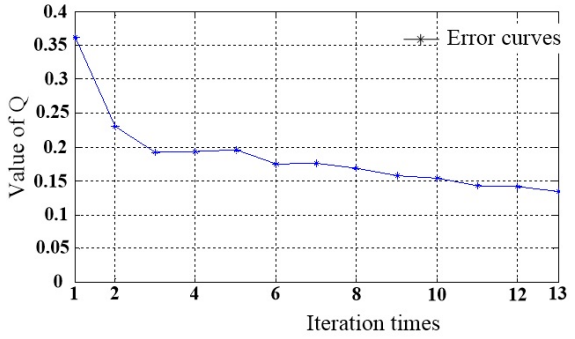

Fig. 7 — Objective function values along with iterations

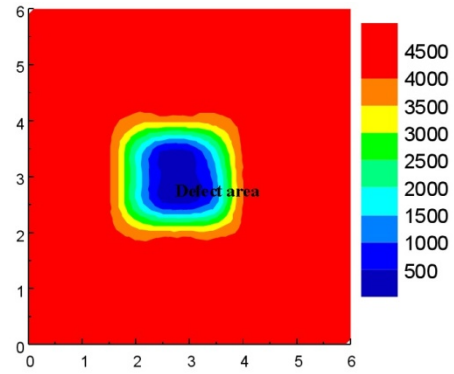

Fig. 9 — Revealed P-wave velocities of the defective model

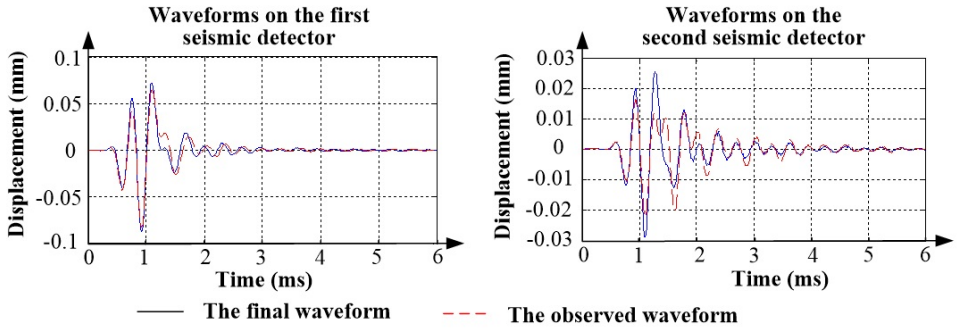

Fig. 8 — Comparison between final and observed waveforms

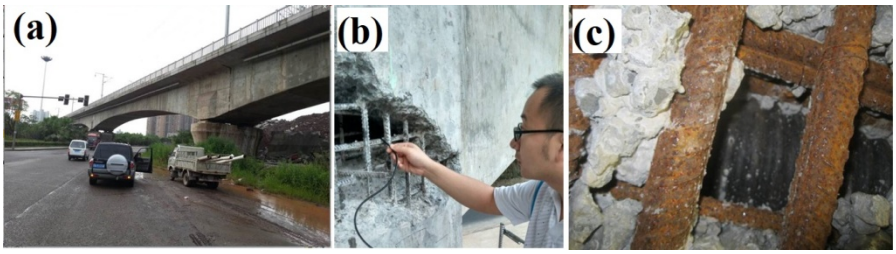

Fig. 10 — a. Photos of the bridge; b. Typical diseases; c. Typical disease details

Fig.11 — field test process: (a). Field data acquisition (receive sensor); (b). Field data acquisition (hammering)

and F2. The other side is receiving acoustic measurement points, numbered S1 and S2. During detection, the F1 and F2 points are successively used as the launching points, and the vibration signals are transmitted by hammering, and each of the transmitting points receives signals at the S1 and S2 receiving points in turn. Inspection section and layout of measuring points are shown in Figure 12 and Figure 13, and the layout of section line is shown in Figure 13.

Concrete waveform inversion imaging test results: The full waveform inversion imaging results are shown in Figure 14. As shown in Figure 14, test results of the three test sections of concrete quality uniformity are as follows:

Profile 1: The wave velocity is generally high, and the average VP of the concrete is 4380 m/s after correction of the area ratio of the section reinforcement. Defects in the areas A, B and C bear seat plate region and the vicinity falls below 3600 m/s, demonstrating the defects of being not dense and regional segregation. Low velocity anomaly areas are: Area A, an area of about 1.3 square meters; Area B , an area of about 2.6 square meters, including 0.3 square meters above the seat; and Area C, an area of

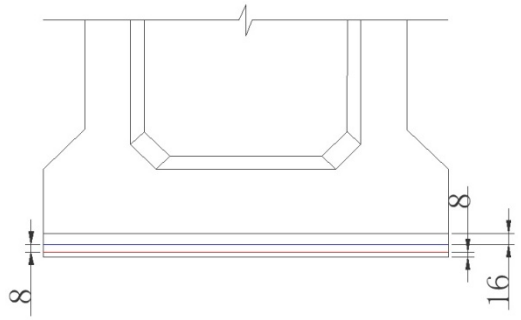

Fig. 12—Test section cross-sectional plan (unit: cm)

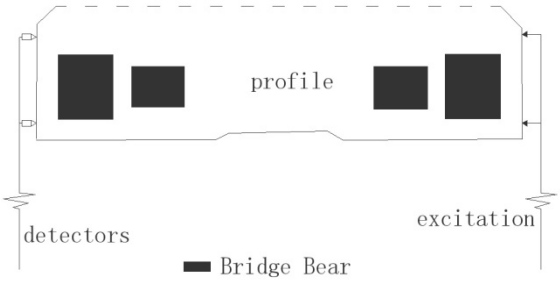

Fig. 13—Test section plan and measuring point layout (unit: cm)

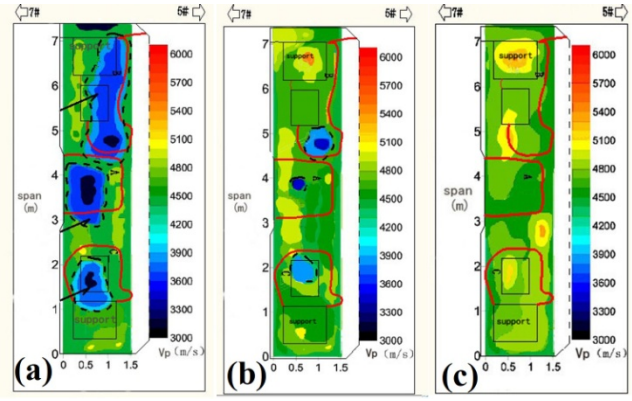

Fig. 14 — Revealed P-wave velocities of inversion: (a) Profile 1; (b) Profile 23; (c) Profile 3.

about 1 square meter, including 0.2 square meter above the seat. The other part of the internal concrete has no obvious quality defects (not dense, segregation or low quality of the concrete, concrete strength grade). Overall, in low velocity anomaly

outside the region reached the strength grade of concrete design requirements.

Profile 2: The test speed is generally high, and the average speed of VP concrete is 4420 m/s. Defects in areas A, B area and C bearing seat plate region and its vicinity fall below 3600 m/s. Low velocity anomaly region VP velocity appeared beam device within the scope of the quality defects of the concrete are (not dense, regional segregation). Low velocity anomaly areas are: Area A, near range area of about 0.1 square meter; Area B near range area of about 0.4 square meter; Area C near the area of about 0.5 square meter. The other part of the internal concrete has no obvious quality defects (not dense, segregation or low quality of the concrete, concrete strength grade). Overall in low velocity anomaly outside the region reached the strength grade of concrete design requirements, and there is no other quality defect.

Profile 3: The testing speed is generally large and the average speed of VP is 4900 m/s after correction according to the area ratio of the section reinforcement. The internal concrete has no obvious quality defects (not dense, segregation or low quality concrete), and the overall strength grade of the internal concrete meets the requirements of the design concrete, and there is no defective zone.

To verify the test results, a borehole endoscope test was carried out in the Area A. When the drilling depth was about 17.5 cm, the concrete density area was reached and the results were in good agreement with the inversion results.

Conclusion

A frequency-domain full waveform inversion method of elastic waves for media is developed to extract quantitative information of elastic properties on subsurface structures. We adopt a quasi-linearization method coupled with a random search algorithm to solve the least-squares problem in inversion, and by this combination, heuristic and non-heuristic inversion methods are designed to complement each other. It is irrelevant to the hypocenter and the hypocenter function used in iteration, confirmed by the frequency spectrum of the observed waveforms.

In Chengdu-Chongqing guest emergency project, the application of full waveform inversion method saves a lot of time. In this method, each section only needs 2 detectors and only need to be hammered twice, while the traditional CT test requires 11 detection filters and at least 11 hammering, and each section has 121 waveform data. In some cases, we can obtain some important priori information through field investigation. The priori information can be used to accelerate the inversion process. Although the full waveform inversion method is 2D, we can obtain 3D information by combining multiple 2D profiles. The efficiency of this method is much higher than that of 3D inversion.

Acknowledgment

The authors would like to express their gratitude to Professor Che of Shanghai Jiaotong University for her helpful advice.

References

1 Plessix, R., Edouard., Introduction: Towards a full waveform inversion, *Geophysical Prospecting*, 56(6) (2008) 761-763.

2 Song, D., Che, A., Chen, Zhu., Ge, X., Seismic stability of a rock slope with discontinuities under rapid water drawdown and earthquakes in large-scale shaking table tests. *Engineering Geology* (245) (2018) 153-168.

3 Song, D., Che, A., Zhu, R., Ge, X., Dynamic response characteristics of a rock slope with discontinuous joints under the combined action of earthquakes and rapid water drawdown, *Landslides*(2) (2017):1-17.

4 Grechka, V., Joint inversion of p- and ps-waves in orthorhombic media: theory and a physical modeling study, *Geophysics,* 64(1) (1999) 146-161.

5 Romdhane, A., Grandjean, G., Brossier, R., Rejiba, F., Operto, S., Virieux, J. Shallow-structure characterization by 2d elastic full-waveform inversion, *Geophysics,* 76(3) (2011) R81-R93.

6 Pan, G.S., Phinney, R.A., Odom, R.I., Full-waveform inversion of plane-wave seismograms in stratified acoustic media: theory and feasibility, *Geophysics,* 53(1) (1988) 21-31.

7 Huston, V., and Pym, J.S. (1980), *Application of functional analysis and operator theory*, New York: Academic Press.

8 Sen, M., Stoffa, P., Nonlinear seismic waveform inversion in one dimension using simulated annealing, *Geophysics,* 56(10) (1990) 1624-1638.

9 Gélis, C., Virieux, J., Grandjean, G. 2d elastic waveform inversion using born and rytov approximations in the frequency domain, *Geophysical Journal International,* 168(2) (2003) 605-633.

10 Beylkin, G., The inversion problem and applications of the generalized radon transform, *Communications on Pure & Applied Mathematics,* 37(5) (1984):579-599.

11 Bae, H., Shin, C., Cha, Y., Choi, Y., Min, D., 2d acoustic-elastic coupled waveform inversion in the laplace domain, *Geophysical Prospecting,* 58(6) (2010) 997–1010.

12 Sun, D., Womersley, R., A new unconstrained differentiable merit function for box constrained variational inequality problems and a damped gauss-newton method, *Siam Journal on Optimization,* 9(2) (2006) 388-413.

13 Sheen, D., Tuncay, K., Baag, C. E., Ortoleva, P., Time domain gauss—newton seismic waveform inversion in elastic media, *Geophysical Journal of the Royal Astronomical Society,* 167(3) (2010) 1373-1384.

14 Zhang, J., Lv, S., Liu, Y., Hu, G., Avo inversion based on generalized extreme value distribution with adaptive parameter estimation, *Journal of Applied Geophysics,* 98(11) (2013) 11-20.

15 Brossier, R., Operto, S., Virieux, J., Seismic imaging of complex onshore structures by 2d elastic frequency-domain full-waveform inversion, *Geophysics,* 74(6) (2009) WCC105.

16 Fu, H., Han, B., A wavelet multiscale method for the inverse problems of a two-dimensional wave equation, *Inverse Problems in Science & Engineering,* 12(6) (2004) 643-656.

17 Barnett, R., Whaley, K., Variational and diffusion monte carlo techniques for quantum clusters, *Physical Review A,* 47(5) (1993) 4082-4098.

18 Sambridge, M., Mosegaard, K., Monte carlo methods in geophysical inverse problems. *Reviews of Geophysics,* 40(3) (2002) 1-29.

19 Rothman, D., Automatic estimation of large residual statics corrections, *Geophysics,* 51(2) (1986) 332-346.

20 Xie, Y., Liu, G., Predicting the distribution of reservoirs by combining variable wavelet model of seismograms with wavelet edge analysis and modeling, *Journal of Applied Geophysics,* 101(101) (2014) 116-123.

21 Pellerin, L., Wannamaker, P., Multi-dimensional electromagnetic modeling and inversion with application to near-surface earth investigations, *Computers and Electronics in Agriculture*, 46 (2005) 71-102,

22 Moya, A., Irikura, K. Inversion of a velocity model using artificial neural networks, *Computers & Geosciences,* 36(12) (2010) 1474-1483.

23 Wang, C., Ma, G., Zhao, J., Soh, C., Identification of dynamic rock properties using a genetic algorithm, *International Journal of Rock Mechanics & Mining Sciences,* 41(3) (2004) 453-453.

24 Zeng, C., Xia, J., Miller, R., Tsoflias, G., Feasibility of waveform inversion of rayleigh waves for shallow shear-wave velocity using a genetic algorithm, *Journal of Applied Geophysics,* 75(4) (2011) 648-655.

25 Song, D., Liang, S., Wang, Z., The influence of reservoir filling on a preexisting bank landslide stability. Indian Journal of Geo-Marine Sciences, 47(2) (2018) 291-300.

26 Yamanaka, H., Comparison of performance of heuristic search methods for phase velocity inversion in shallow surface wave method, *Journal of Environmental & Engineering Geophysics,* 10(2) (2012) 163-173.

27 Song, D., Dong, L., Feng, X., Approach to the application of ultrasonic technology to measuring physical properties of new building materials, *Indian Journal of Geo-Marine Sciences*, 48(5) (2019) 739-746.

28 Ernst, J., Green, A., Maurer, H., Holliger, K., Application of a new 2d time-domain full-waveform inversion scheme to crosshole radar data, *Geophysics,* 72(5) (2007) J53-J64.

29 Askan, A., Akcelik, V., Bielak, J., Ghattas, O., Parameter sensitivity analysis of a nonlinear least-squares optimization-based anelastic full waveform inversion method, *Comptes Rendus Mécanique,* 338(7–8) (2010) 364-376.

30 Lampe, J., Voss, H., Large-scale Tikhonov regularization of total least squares, *Journal of Computational and Applied Mathematics*, Vol. 238 (2013) 95-108.

31 Kumar, R., Kabamba, P., Hyland, D., Analysis and parameter selection for an adaptive random search algorithm, *Mathematics & Computers in Simulation,* 68(2) (2005) 95-103.

32 Chew, W.C. and Liu, Q.H. Perfectly matched layers for elastodynamics: A new absorbing boundary condition, *Journal of Computational Acoustics*, 4 (1996) 341-359.

33 Kaltenbacher, B., Kaltenbacher, M., Sim, I., A modified and stable version of a perfectly matched layer technique for the 3-d second order wave equation in time domain with an application to aeroacoustics, *Journal of Computational Physics,* 235(100) (2013) 407-422.